Effect of Chirality and Length on the Penetrability of Single-Walled Carbon Nanotubes into Lipid Bilayer Cell Membranes

ARTICLE *in* LANGMUIR · APRIL 2012

Impact Factor: 4.46 · DOI: 10.1021/la3011162 · Source: PubMed

3 AUTHORS:

Amir alipour skandani
University of Pittsburgh
13 PUBLICATIONS **39** CITATIONS
SEE PROFILE

Reema Zeineldin
Massachusetts College of Pharmacy and Healt…
18 PUBLICATIONS **414** CITATIONS
SEE PROFILE

Marwan Al-Haik
Embry-Riddle Aeronautical University
116 PUBLICATIONS **1,050** CITATIONS
SEE PROFILE

Langmuir

Article

pubs.acs.org/Langmuir

Effect of Chirality and Length on the Penetrability of Single-Walled Carbon Nanotubes into Lipid Bilayer Cell Membranes

A. Alipour Skandani,[†] R. Zeineldin,[‡] and M. Al-Haik*,[†]

[†]Department of Engineering Science and Mechanics, Virginia Tech, Blacksburg, Virginia 24061, United States

[‡]Department of Pharmaceutical Sciences, Massachusetts College of Pharmacy & Health Sciences, Worcester, Massachusetts 01608, United States

Supporting Information

ABSTRACT: The ability of carbon nanotubes to enter the cell membrane acting as drug-delivery vehicles has yielded a plethora of experimental investigations, mostly with inconclusive results because of the wide spectra of carbon nanotube structures. Because of the virtual impossibility of synthesizing CNTs with distinct chirality, we report a parametric study on the use of molecular dynamics to provide better insight into the effect of the carbon nanotube chirality and the aspect ratio on the interaction with a lipid bilayer membrane. The simulation results indicated that a single-walled carbon nanotube utilizes different time-evolving mechanisms to facilitate their internalization within the membrane. These mechanisms comprise both penetration and endocytosis. It was observed that carbon nanotubes with higher aspect ratios penetrate the membrane faster whereas shorter nanotubes undergo significant rotation during the final stages of endocytosis. Furthermore, nanotubes with lower chiral indices developed significant adhesion with the membrane. This adhesion is hypothesized to consume some of the carbon nanotube energy, thus resulting in longer times for the nanotube to translocate through the membrane.

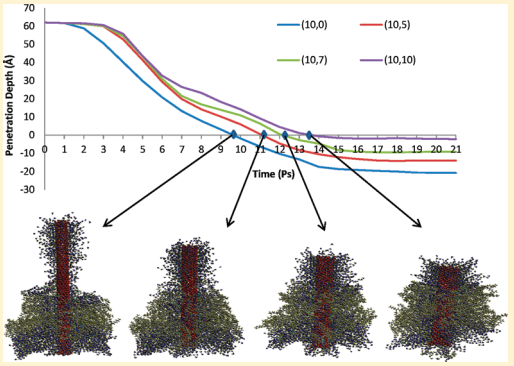

INTRODUCTION

The introduction of nanomaterials into the biomedical and biotechnological fields had opened a plethora of applications that were not possible before. The need to understand the interaction of engineered nanomaterials with live organs, in particular, their effect on human health, has been a pressing challenge.[1−3] Also, their potential to enhance both the determination of and medication for several terminal diseases such as cancer, tumors, and so on is of great interest and currently is the topic of several ongoing investigations.[4−6]

Several emerging technologies seek to employ nanomaterials as vehicles to deliver molecular probes and drugs into the cell. Carbon nanostructures and, in particular, carbon nanotubes (CNTs) are attracting growing attention for therapeutic active molecule delivery. It has been demonstrated that CNTs are capable of delivering proteins,[7] peptides,[8] and nucleic acids[9] to different cells. Single-walled carbon nanotubes (SWCNTs) are promising candidates for invasive cancer treatments such as photothermal therapies because of their high near-infrared absorption and for drug delivery because of their high diffusivity into cells.[4,5] Furthermore, the photoacoustic properties of SWCNTs are utilized for targeting and the selective destruction of cancer cells.[10]

Despite all of these plausible properties of CNTs, several issues relating to their toxicity and the mechanism by which CNTs interact with the cell membranes need to be explored further.[11] For example, the in vitro toxicity of SWCNTs is not yet fully determined, which can be mostly attributed to the broad variations in the synthesis and purification methods[1] of these materials. Postprocessing can also alter the toxicity of SWCNTs. It was reported that functionalized CNTs display low toxicity and could be modified to be nonimmunogenic.[12]

Although the CNTs were detected via different means (e.g., transient absorption microscopy,[13] Raman spectroscopy,[14] and confocal microscopy[4]) to be able to pass through the cell membranes, the mechanisms of the translocation of the CNTs through the phospholipid bilayers and their penetration into cells are yet to be determined. Several hypotheses were developed to explain the mechanism by which CNTs can translocate through cell membranes. The competing scenarios include nonspecific physical penetration,[15] endocytosis,[16,17] and spontaneous thermally driven diffusion across the cell membrane.[18,19]

Kostareols et al.[20] concluded that functionalized carbon nanotubes (f-CNTs) possess the capacity to traffic intracellularly through the different cellular barriers by energy-independent mechanisms. The cylindrical shape and the high aspect ratio of f-CNTs can allow their penetration through the plasma membrane, similar to a nanosyringe.[20] Alternatively, Yaron et al.[17] attributed the internalization of CNTs into cells

Received: March 15, 2012
Revised: April 26, 2012
Published: April 30, 2012

to energy-dependent endocytosis. In contradiction, some theoretical investigations provided results indicating that because of their small diameters CNTs may not be able to initiate endocytosis.[16]

Because of the conflicting findings of several experimental studies, computer simulations were sought to investigate the mechanics of nanotube translocation through lipid membranes. Early investigations focused on the spherical form of carbon (fullerenes) interaction with lipid membranes and emphasized the importance of functionalizing the surface to facilitate their adsorption onto bilayer membrane.[21] More recent investigations emphasized the effect of the shape of the particles, their anisotropy, and their initial orientation to be crucial to the nature of the interaction between the particle and the lipid bilayer. In particular, the contact area between the particle and lipid and the local curvature of the particle at the contact point are key parameters that trigger the translocation.[22]

Several studies employed a molecular dynamics (MD) simulation to investigate the interaction of CNTs with lipid membranes. Wallace and Sansom[23] used coarse-grained molecular dynamics to simulate the penetration of dipalmitoylphosphatidylcholine (DPPC) bilayers by SWCNTs. The simulation showed the lipid lining the inner surface of the CNTs, which suggested that for drug-delivery applications the therapeutic molecule should be attached to the exterior of the nanotube. Pogodin and Baulin[18] utilized single-chain mean field theory to calculate the energy required to insert a single CNT into the phospholipid bilayer, and they found that the energy cost of the bilayer rupture is quite high compared to that of the energy of thermal motion. This conclusion indirectly supports other energy-dependent translocation mechanisms such as endocytosis.

Experimental findings by the authors of this article[24] and simulation by another group[23] concluded that the length and diameter of a CNT are deterministic parameters for how far a CNT can travel through cell membranes. Although there are numerous publications employing molecular dynamics to simulate the mechanics of CNTs/lipid interaction, fewer investigations took into account the geometry of the CNTs such as the length. Moreover, a majority of the published efforts assume a single type of CNTs and neglect a very crucial parameter; the chirality of the CNTs.

Understandably, it is rather hard, if not impossible, to grow CNTs with distinct chirality. Furthermore, extracting and isolating CNTs out of a bundle based on their chiralities is still in its infancy.[25−28] Therefore, because of the lack of a reasonable method to narrow down the chirality distribution of SWCNTs, experimental parametric investigations of how the chirality affects the CNTs interaction with cell membranes are currently unavailable.

The purpose of this investigation is to clarify the effect of the length and chirality on the dynamic translocation of SWCNTs through a bilayer phospholipid membrane. To this end, we carried out MD simulations for four different SWCNT chiralities with two different lengths. We also studied the interaction between the nanotube and the membrane qualitatively by probing the possibility of adhesion between the two entities. These simulations shed some light on the effect of CNT morphology on their translocation into cells that could facilitate future efforts toward tailoring the cell uptake of CNTs toward delivering specific quantities of therapeutic molecules or bioprobes.

CHIRALITY IN SWCNT

The chirality, defined by the chiral vector $\vec{C}_h$ and the chiral angle θ (briefly described here for completeness), characterizes the atomic structure of an SWCNT. They are also called the roll-up vector (that defines its diameter) and the helical angle, respectively. The chiral vector, $\vec{C}_h = n\vec{a}_1 + m\vec{a}_2$, is defined on the honeycomb lattice of carbon atoms by unit vectors $\vec{a}_1$ and $\vec{a}_2$ (shown in Figure 1) and the integers (n, m) that represent the

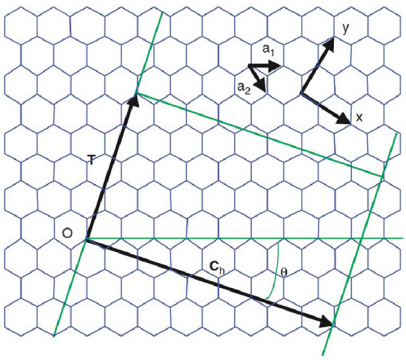

Figure 1. Illustration of the chiral angle and chiral vector.

number of steps along the zigzag carbon bonds of the hexagonal lattice. The chiral angle is the smallest angle enclosed by the nanotube axis and the row of edge-sharing hexagons, or, in other words, the smallest angle between the circumference line (chiral vector) and the primitive lattice vector (zigzag direction) on the hexagonal sheet as shown in Figure 1. A single-walled carbon nanotube can be visualized as a sheet of graphite, marked by bold lines in Figure 1, rolled into a tube such that the tip of the chiral vector touches its tail. The nanotube configurations where the chiral angles assume the extreme values of 0 and 30° are the limiting cases referred to as "zigzag" and "armchair", respectively. In terms of the chiral vector, the zigzag nanotube is defined as $(n, 0)$, and the armchair nanotube, as (n, n). The chiral angle θ may be viewed as a measure of the twist in the tube, and this chirality dictates the nanotube diameter.[24]

Single-walled carbon nanotubes can also be defined with diameter D_n and chiral angle θ, which themselves can be obtained uniquely by the integer pair (n, m)

$$\theta = \pi \tan^{-1}\left(\frac{\sqrt{3}m}{2n + m}\right) \quad (1)$$

$$D_n = \frac{\sqrt{3}}{\pi} b\sqrt{n^2 + m^2 + nm} \quad (0 \le m \le n) \quad (2)$$

where b is the C−C bond length (0.142 nm). The thermal,[29] electronic,[30] and mechanical[31] properties of SWCNTs vary substantially depending on the SWCNT diameters and chiral angles.

FORCE FIELD SELECTION

The CHARMM27[32,33] all-atom force field represents a highly optimized empirical model that is valid for investigating nucleic acids, proteins, and lipids, allowing for simulation studies of heterogeneous systems via empirical force field calculations.[34,35]

dx.doi.org/10.1021/la3011162 | Langmuir 2012, 28, 7872−7879

Equation 3 describes the functional form of the potential energy calculated by CHARMM27

$$E = \sum_{\text{bonds}} k_b(b - b_0)^2 + \sum_{\text{UB}} k_{\text{UB}}(S - S_0)^2 + \sum_{\text{angles}} k_\theta(\theta - \theta_0)^2 + \sum_{\text{dihedrals}} k_\varnothing[1 + \cos(n\varnothing - \delta)] + \sum_{\text{impropers}} k_\omega(\omega - \omega_0)^2 + \sum_{\text{nonbond}} \in \left[\left(\frac{R_{\min ij}}{\tau_{ij}}\right)^{12} - \left(\frac{R_{\min ij}}{\tau_{ij}}\right)^{5}\right] + \frac{q_i q_j}{\in_1 \tau_{ij}} \quad (3)$$

where K_b, K_{UB}, K_θ, K_ϕ, and K_ω are the bond, Urey–Bradley, angle, dihedral angle, and improper dihedral angle force constants, respectively; b, S, θ, ϕ, and ω are the bond length, Urey–Bradley 1,3 distance, bond angle, dihedral angle, and improper torsion angle, respectively, with the subscript zero representing the equilibrium values for the individual terms. In the dihedral term, n is the multiplicity and δ is the phase, which dictates the location of the minima and maxima. Coulomb and Lennard-Jones 6–12 terms contribute to the external or nonbonded interactions; $\in$ is the Lennard-Jones well depth, $R_{\min}$ is the distance at the Lennard-Jones minimum, q_i is the partial atomic charge, $\in_1$ is the effective dielectric constant, and r_{ij} is the distance between atoms i and j.[35] Numerous investigations with adaptive improvements have turned CHARMM27 into one of the most utilized force fields for MD simulations of biomolecules.[34−37]

NUMERICAL EXPERIMENTS

The membrane cell in the current study comprises 72 dimyristoyl-*sn*-glycerophosphatidylcholine (DMPC) lipids, a common membrane lipid,[38,39] and 2716 water molecules, making an overall 17 796 atom structure. To investigate the effect of chirality and length separately, eight SWCNT configurations were assembled. The morphologies comprised four short SWCNTs with (10, 0), (10, 5), (10, 7), and (10, 10) chirality indices. Four longer nanotubes, double the length of the short ones, with identical chiralities were generated to investigate the effect of the nanotube length on translocation through the membrane.

To ensure the applicability of the CHARMM27 force field to both constituents, we analyzed the C–C bond in the lipid chains, the C–C bond within the body of the tubes, and the C–C bonding at the open ends of the SWCNTs. We noticed significant difference between the behavior of the carbon atoms located at the ends and at the body of the SWCNT. The number of nearest neighbors (only 2) at the SWCNT open ends is less than that for the body atom (3), and carbon atoms at the ends are unsaturated. The unsaturated boundary effect can be avoided by adding hydrogen atoms to the open ends of the CNT.[40,41] This practice in effect accounts for the cap effect of the CNTs and was reasonably employed by several groups.[41,42] The exact numbers of carbon and hydrogen atoms for each chiral nanotube are presented in Table 1.

Upon investigating the force field compatibility for this enforced C–H bonding, we found that the "standard" CHARMM27 force field does not account for two missing bending angle parameters between the carbon atoms of nanotube and the added hydrogen. Because these force fields are largely empirical, we assigned the appropriate values for these two parameters from analogous C–H bond types in a classical force field—the molecular mechanics (MM3) force field. The MM3 force field is mostly used for hydrocarbon structures[43−45] rather than biomolecules.

Table 1. Total Number of Atoms Utilized in MD Simulation for Chiral Nanotubes

		H atoms	C atoms	nanotube diameter (nm)	nanotube length (nm)	chiral angle θ°
(10,0) NT-zigzag	short	40	600	0.783	6.5541	0.00
	long		1280		13.472	
(10,5) NT	short	50	600	1.036	5.2281	19.11
	long		1300		10.972	
(10,7) NT	short	54	600	1.158	4.8061	24.18
	long		1308		10.212	
(10,10) NT-armchair	short	60	600	1.356	4.1278	30.00
	long		1320		8.932	

Having passed the force field compatibility test, the functionalized SWCNTs were individually placed above the center of mass of the membrane aligned with its Z axis. A 2 Å clearance was maintained in all configurations, preventing the tube from interacting with the membrane while carrying out the minimization step.

The simulations were carried out using TINKER, a general purpose package of molecular dynamics simulation subroutines.[46] Prior to the dynamics step, all of the numerically generated microstructures were relaxed through the numerical minimization of the potential energy with a BFGS quasi-Newton algorithm to a convergence criterion where the rms per atom force cutoff of the energy is equal to or less than 1 kcal/mol Å. For example, for a long (10, 5) SWCNT the initial simulation box dimensions were set to approximately 109.009 × 24.713 × 14.145 Å^3, and upon the relaxation of the molecule, the simulation box size was found to be 113.000 × 28.000 × 16.000 Å^3. The individual SWCNTs and the membrane were minimized both before and after assembling them.

The assembled SWCNT/membrane simulation cells were obtained by equilibrating the system after combining the two structures. This equilibration is conducted by enforcing Newton's equation of motion

$$F_i = m_i \frac{d^2 r_i}{dt^2} = -\partial \frac{E(r_1, r_2, ..., r_N)}{\partial r_i} \quad (4)$$

where m_i is the atomic mass of the ith atom. Successive configurations of the system are generated by the time integration of eq 3. The result is a trajectory that specifies how the positions and velocities of the particles in the system vary with time. A statistical ensemble is used to compute the average of the physical quantity of interest. The physical quantity is taken as the time average on the trajectory. Statistical mechanics relates MD averages to their thermodynamic counterparts, and the ergodicity hypothesis can be invoked to justify equating the trajectory averages to ensemble-based thermodynamic properties.[47,48]

For each SWCNT/membrane system, we conduct a molecular dynamics simulation for 60 ps with an MD time step of 1.0 fs under a constant temperature of 300 K and an external pressure of 1.0 atm. Unlike previous investigations,[23] we did not apply steered molecular dynamics (SMD) where an explicit external velocity is imposed to pull the nanotube through the bilayer. Rather, we relied on the statistical thermodynamics ensembles to rescale the velocities of the

dx.doi.org/10.1021/la3011162 | Langmuir 2012, 28, 7872–7879

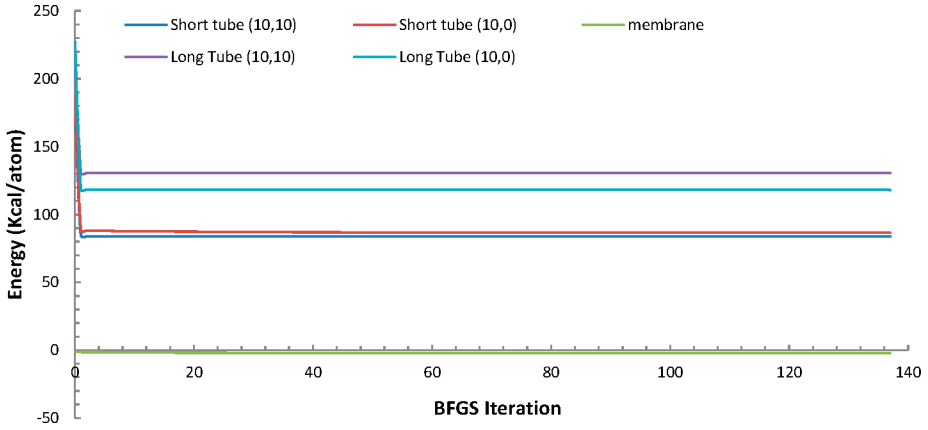

Figure 2. Energy minimization for the different SWCNTs and the bilayer membrane.

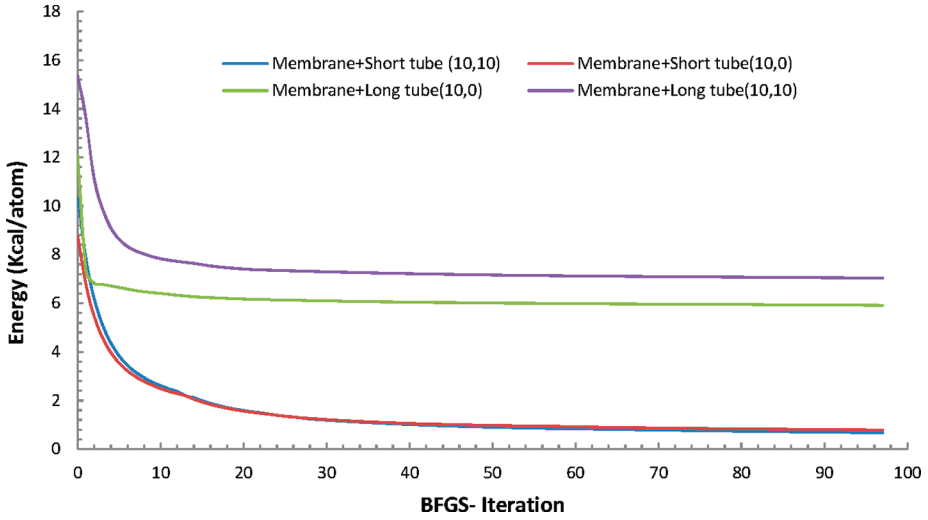

Figure 3. Energy minimization data for some of the SWCNT/membrane assembled configurations.

system particles to achieve thermodynamic equilibrium. This scenario is closer to most of the experimental investigations mentioned earlier; no external field was applied to enforce the CNT translocation within the membrane.

All of the MD simulations were performed within the framework of the canonical statistical ensemble (*NVT*), which is characterized by a fixed number of atoms, *N*, a fixed volume, *V*, and a fixed temperature, *T*. A Berendsen thermostat was used for temperature control in the box. The numerical integration of the equation of motion was performed using the velocity Verlet algorithm. The integration time step was 1.0 fs, and the cutoff distance for the 12−6 Lennard-Jones potential was set to 9.0 Å.

RESULTS AND DISCUSSION

Plotted in Figures 2 and 3 are the minimum potential energies per atom for the relaxed individual SWCNTs and the bilayer membrane achieved through the LM-BFGS minimization algorithm.

The chirality seems not to influence the change in the potential energy for the short nanotubes as much as the nanotube length does. Doubling the length of the nanotube increased the equilibrium potential energy of the membrane/CNT systems by 3-fold (Figure 3).

Effect of the SWCNT Length. The relaxed SWCNT/membrane systems were further equilibrated by conducting MD simulation guided by an *NVT* ensemble. The evolution of the potential energy for the two systems based on short and long zigzag and armchair nanotube systems is shown in Figures 4 and 5, respectively. The relation between the approximation inherent in the velocity Varlet integration algorithm and the fluctuation in potential energy are discussed by Leach,[48] where he indicates that a variation of the potential energy in the range of 0.001−0.01 kcal/atom is generally considered to be acceptable as an equilibrium criterion. Because the change in potential energy beyond 60 ps is found to be about 0.004 kcal/atom, the system could be reasonably assumed to have reached equilibrium. Therefore, in the interest of computational time, the simulations were terminated at 60 ps.

Although the number of atoms is almost identical, regardless of the length, SWCNTs with smaller chiral indices (zigzag) always attained the highest total energy because its slenderness allows more interactions with the membrane during the dynamic simulations. Increasing the length further contrasted with this observation (Figure 5) as the SWCNT aspect ratio doubled.

Investigating the trajectories of the different configurations at the different peaks in the energy evolution curves (the energy

dx.doi.org/10.1021/la3011162 | *Langmuir* 2012, 28, 7872−7879

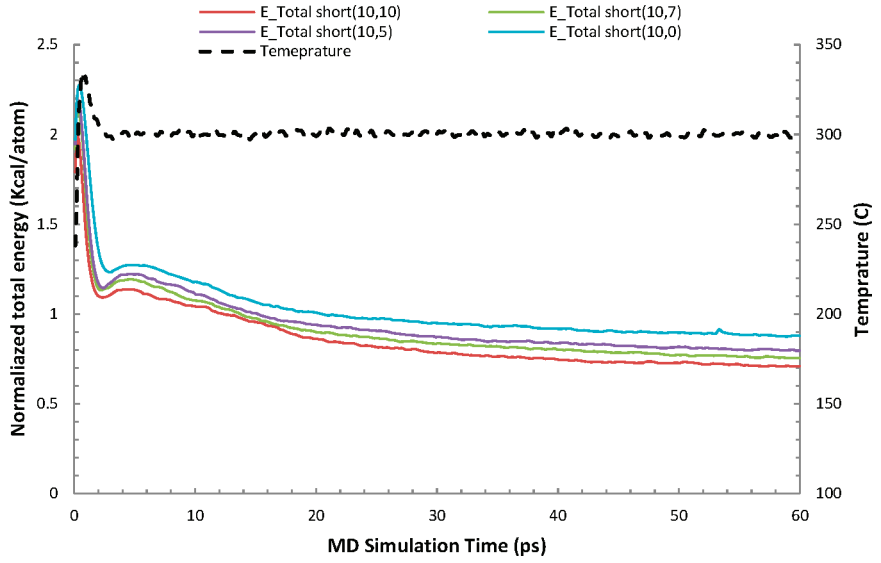

Figure 4. Total energy and temperature evolutions during the molecular dynamic simulation of short nanotubes.

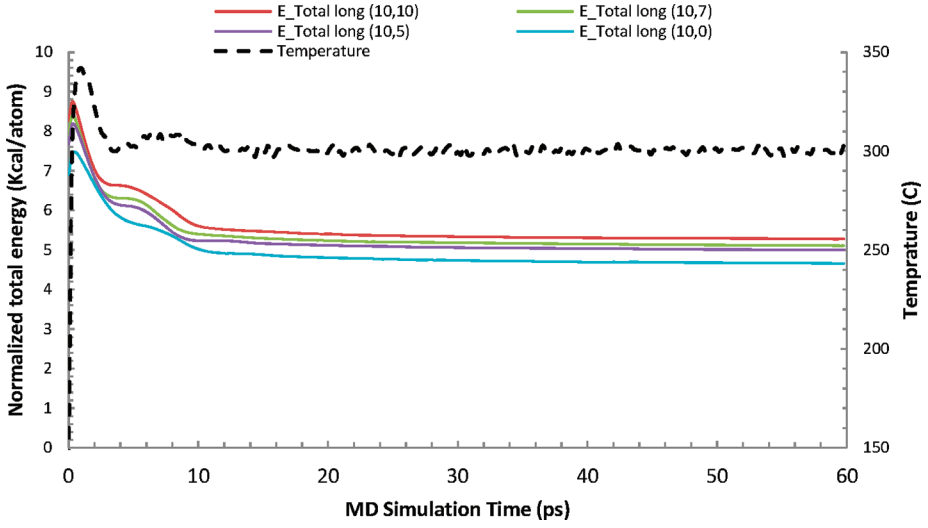

Figure 5. Total energy and temperature evolutions during the molecular dynamic simulation of long nanotubes.

peaks in Figure 5) can provide useful insight into the SWCNT/membrane interactions. Figure 6 shows several MD snapshots at different simulation times for the eight SWCNT/membrane configurations. The first observation is that the mechanism of insertion comprises pure penetration at early stages (times within 0.4 ps) and a mix of penetration and endocytosis in between 0.4 and 10 ps that is mostly dominated by endocytosis in the later stages (10−60 ps).

When we hold the chirality constant, longer nanotubes find their way through the membrane faster with less rotation from the vertical position. On the contrary, tubes with length shorter than the thickness of a membrane (i.e., ∼60 Å) are more likely to rotate in the membrane while trafficking via the endocytosis mechanism. The rotation of short nanotubes in relatively thick membranes was previously reported.[49]

These observations highlight the importance of the size of the membrane relative to the CNT length. Undoubtedly, if the membrane is large enough, the longer CNTs will end up being surrounded by the membrane as well. Because the rotation is a 3-D process that is also time-dependent and the CNT is not rigid (i.e., outside walls will undergo some deformation because of the interactions with the membrane walls), these issues will induce several parameters to quantify the overall rotations and correlate it to the chirality.

■ EFFECT OF CHIRALITY

Long SWCNTs were chosen to probe the chirality effect. Figure 7 shows the trajectory of the bottommost carbon atom, of each SWCNT, from the starting point (i.e., z = ∼62 Å) to complete insertion when the SWCNT's lower end moves out of the second layer of the membrane (i.e., z = 0 Å). The results suggest that SWCNTs with lower chirality indices and aspect ratio penetrate faster. However, wider and shorter tubes, with larger surface interactions, tend to rotate.

■ ADHESION

The adhesion energy is estimated as the difference between the potential energy of the SWCNT/membrane system and the sum of the potential energies for the membrane and the corresponding SWCNT: $\Delta E = E_{total} - (E_{CNT} + E_M)$, where E_{total} is the total potential energy of the integrated cell

dx.doi.org/10.1021/la3011162 | Langmuir 2012, 28, 7872−7879

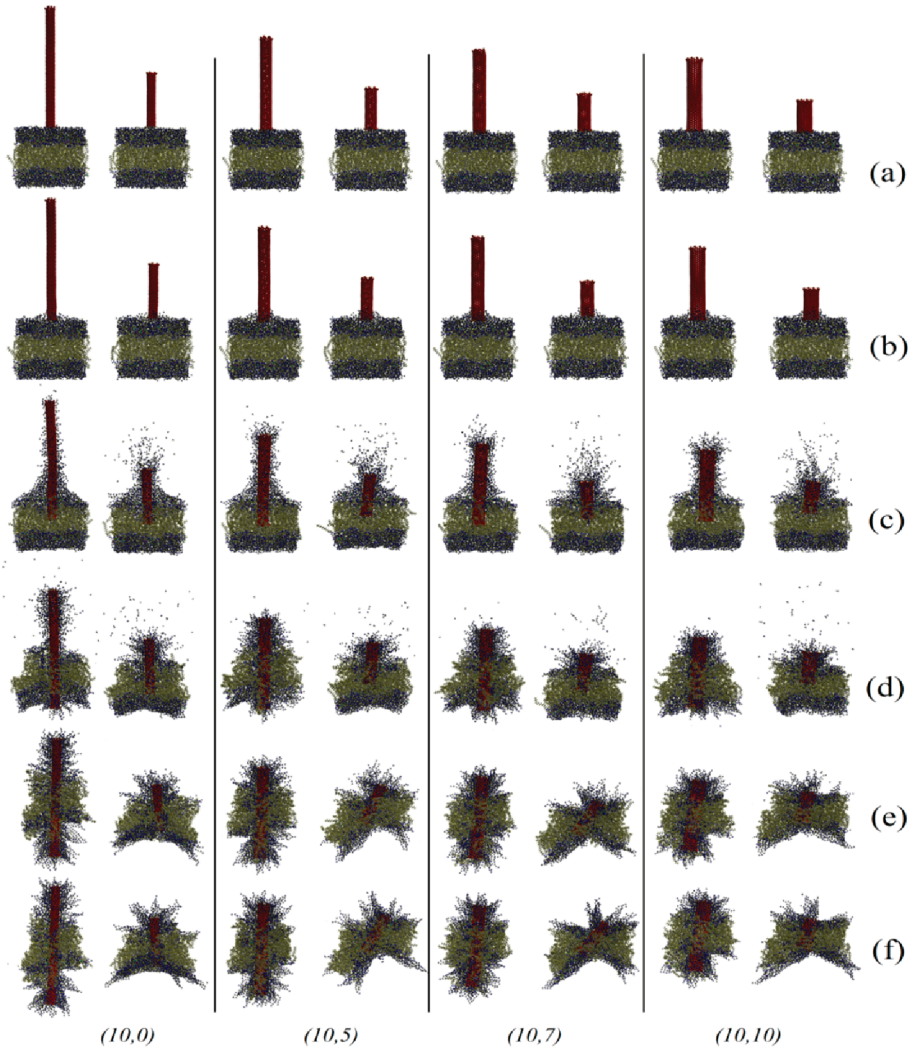

Figure 6. Sequential representation of SWCNT penetration through the cell membrane: (a) initial configuration, (b) after 0.4 ps, (c) after 4 ps, (d) after 10 ps, (e) after 30 ps, and (f) after 60 ps.

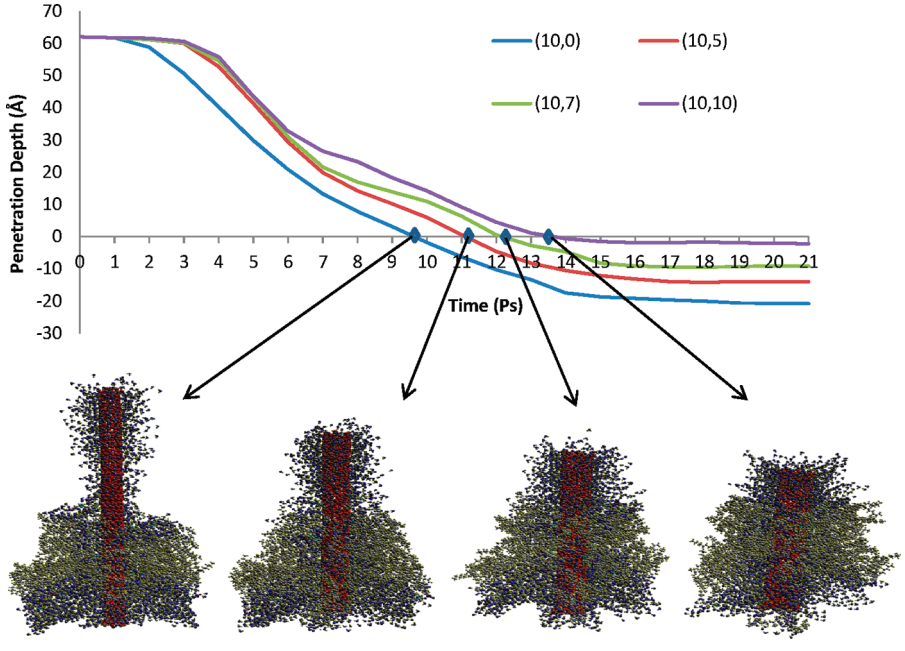

Figure 7. Molecular dynamic evolution of the z coordinate of the bottommost carbon atom in different chiralities.

dx.doi.org/10.1021/la3011162 | *Langmuir* 2012, 28, 7872−7879

comprising SWCNT/membrane at the end of equilibration, E_{CNT} is the potential energy of the nanotube alone, and E_M is the potential energy of the membrane alone. Both E_{CNT} and E_M were precalculated via separate MD simulations using the *NVT* ensemble to calculate the final potential energy after 60 ps.

Figure 8 depicts the adhesion energy per atom of the different membrane/CNT configurations versus the corresponding chirality of the nanotube. Obviously, for the same chiral indices, system based on longer SWCNTs will attain a higher adhesion energy merely for the increased surface area. It is clear that the adhesion energy attains the highest value for the armchair system whereas the zigzag nanotube system achieves the least adhesion energy. These results can be better understood by referring to Figure 6. By the end of the 60 ps, all of the short nanotubes regardless of their chirality were completely surrounded by the membrane and thus all of them create more or less equivalent interactions with the membrane. However, upon doubling the lengths of the CNTs, nanotubes with higher chiralities (e.g., (10, 10) and (10, 7)) were completely surrounded by the membrane by the end of the 60 ps whereas those with lesser chiralities (e.g., (10, 0)) were partially encapsulated and thus encountered partial interactions with the membrane, leading to lesser adhesion. Hence, a higher-chirality SWCNT establishes more interaction (mostly VW and coulombic) with the membrane, leading to better adhesion.

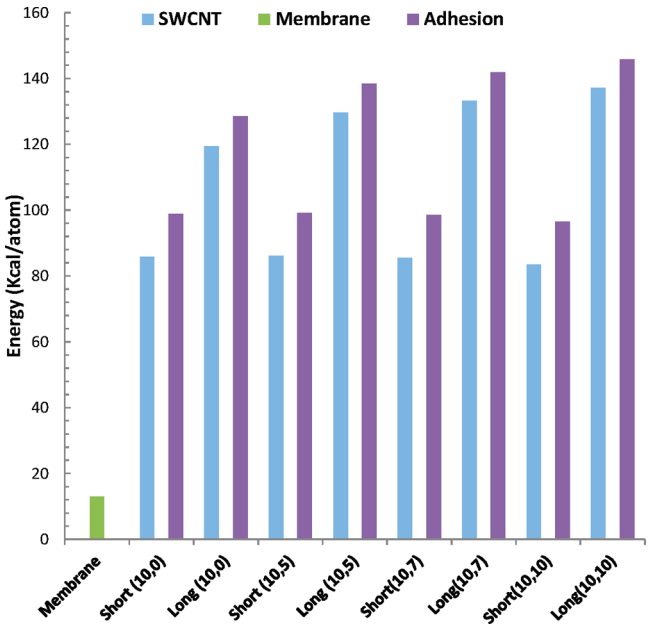

Figure 8. Adhesion energy of the different SWCNTs/membrane configurations.

CONCLUSIONS

In the present study, molecular dynamic simulations were employed to understand the effects of chirality and length on the translocation of SWCNTs into a lipid bilayered cell membrane. The simulations revealed that for the earliest time spans the mechanism of interaction between the SWCNT and the membrane is pure penetration. As time evolves, penetration is accompanied by endocytosis, and almost halfway through 60 ps, endocytosis becomes the dominant form of interaction.

This study also showed that shorter nanotubes, with lengths less than the thickness of the membrane, undergo significant rotation during the endocytosis stage. By doubling the length, all of the SWCNTs penetrated the membrane and the chirality showed its effect vividly. Lower chirality (a higher aspect ratio) assisted the SWCNT in crossing the membrane faster. This was also concluded from the weaker adhesion established between the membrane and the SWCNT with the lowest chirality, (10, 0). Because less of the SWCNT energy was consumed to establish adhesion with the membrane, it was capable of translocating through the membrane from the other side faster than the other nanotubes.

ASSOCIATED CONTENT

Supporting Information

Animation for the penetration of all studied configurations. This material is available free of charge via the Internet at http://pubs.acs.org.

AUTHOR INFORMATION

Corresponding Author

*E-mail: alhaik@vt.edu.

Notes

The authors declare no competing financial interest.

ACKNOWLEDGMENTS

This work has been supported by National Science Foundation (NSF) award CMMI: CAREER -0846589 to M.A.-H. We gratefully acknowledge this support.

REFERENCES

(1) Becker, M. L.; Fagan, J. A.; Gallant, N. D.; Bauer, B. J.; Bajpai, V.; Hobbie, E. K.; Lacerda, S. H.; Migler, K. B.; Jakupciak, J. P. Length-dependent uptake of DNA-wrapped single-walled carbon nanotubes. *Adv. Mater.* **2007**, *19*, 939−945.

(2) Warheit, D. What is currently known about the health risks related to carbon nanotube exposures? *Carbon* **2006**, *44*, 1064−1069.

(3) Smart, S.; Cassady, A.; Lu, G.; Martin, D. The biocompatibility of carbon nanotubes. *Carbon* **2006**, *44*, 1034−1047.

(4) Zeineldin, R.; Al-Haik, M.; Hudson, L. G. Role of polyethylene glycol integrity in specific receptor targeting of carbon nanotubes to cancer cells. *Nano Lett.* **2009**, *9*, 751−757.

(5) Zhou, F.; Xing, D.; Ou, Z.; Wu, B.; Resasco, D. E.; Chen, W. R. Cancer photothermal therapy in the near-infrared region by using single-walled carbon nanotubes. *J. Biomed. Opt.* **2009**, *14*, 021009.

(6) Kohli, P.; Martin, C. R. Smart nanotubes for biotechnology. *Curr. Pharm. Biotechnol.* **2005**, *6*, 35−47.

(7) Li, C. Y.; Yang, K. Q.; Zhang, Y. Y.; Tang, H.; Yan, F.; Tan, L.; Xie, Q. J.; Yao, S. Z. Highly biocompatible multi-walled carbon nanotube-chitosan nanoparticle hybrids as protein carriers. *Acta Biomater.* **2011**, *7*, 3070−3077.

(8) Villa, C. H.; Dao, T.; Ahearn, I.; Fehrenbacher, N.; Casey, E.; Rey, D. A.; Korontsvit, T.; Zakhaleva, V.; Batt, C. A.; Philips, M. R.; Scheinberg, D. A. Single-walled carbon nanotubes deliver peptide antigen into dendritic cells and enhance igg responses to tumor-associated antigens. *ACS Nano* **2011**, *5*, 5300−5311.

(9) Varkouhi, A. K.; Foillard, S.; Lammers, T.; Schiffelers, R. M.; Doris, E.; Hennink, W. E.; Storm, G. SiRNA delivery with functionalized carbon nanotubes. *Int. J. Pharm.* **2011**, *416*, 419−425.

(10) Kang, B.; Yu, D.; Dai, Y.; Chang, S.; Chen, D.; Ding, Y. Cancer-cell targeting and photoacoustic therapy using carbon nanotubes as "bomb" agents. *Small* **2009**, *5*, 1292−1301.

(11) Gogotsi, Y. How safe are nanotubes and other nanofilaments? *Mater. Res. Innov.* **2003**, *7*, 192−194.

(12) Roda, E.; Coccini, T.; Acerbi, D.; Barni, S.; Vaccarone, R.; Manzo, L. Comparative pulmonary toxicity assessment of pristine and functionalized multi-walled carbon nanotubes intratracheally instilled in rats: morphohistochemical evaluations. *Histol. Histopathol.* **2011**, *26*, 357−367.
(13) Tong, L.; Liu, Y. X.; Dolash, B. D.; Jung, Y.; Slipchenko, M. N.; Bergstrom, D. E.; Cheng, J. X. Label-free imaging of semiconducting and metallic carbon nanotubes in cells and mice using transient absorption microscopy. *Nat. Nanotechnol.* **2012**, *7*, 56−61.
(14) Niu, J. J.; Schrlau, M. G.; Friedman, G.; Gogotsi, Y. Carbon nanotube-tipped endoscope for in situ intracellular surface-enhanced Raman spectroscopy. *Small* **2011**, *7*, 540−545.
(15) Vakarelski, I. U.; Brown, S. C.; Higashitani, K.; Moudgil, B. M. Penetration of living cell membranes with fortified carbon nanotube tips. *Langmuir* **2007**, *23*, 10893−10896.
(16) Gao, H.; Shi, W.; Freund, L. B. Mechanics of receptor-mediated endocytosis. *Proc. Natl. Acad. Sci. U.S.A.* **2005**, *102*, 9469−9474.
(17) Yaron, P. N.; Holt, B. D.; Short, P. A.; Lösche, M.; Islam, M. F.; Dahl, K. N. Single wall carbon nanotubes enter cells by endocytosis and not membrane penetration. *J. Nanobiotechnol.* **2011**, *9*, No. 45.
(18) Pogodin, S.; Baulin, V. A. Can a carbon nanotube pierce through a phospholipid bilayer? *ACS Nano* **2010**, *4*, 5293−5300.
(19) Lu, Q.; Moore, J. M.; Huang, G.; Mount, A. S.; Rao, A. M.; Larcom, L. L.; Ke, P. C. RNA polymer translocation with single-walled carbon nanotubes. *Nano Lett.* **2004**, *4*, 2473−2477.
(20) Kostarelos, K.; Lacerda, L.; Pastorin, G.; Wu, W.; Wieckowski, S.; Luangsivilay, J.; Godefroy, S.; Pantarotto, D.; Briand, J.-P.; Muller, S.; Prato, M; Bianco, A. Cellular uptake of functionalized carbon nanotubes is independent of functional group and cell type. *Nat. Nanotechnol.* **2007**, *2*, 108−113.
(21) Qiao, R.; Roberts, A. P.; Mount, A. S.; Klaine, S. J.; Ke, P. C. Translocation of C60 and its derivatives across a lipid bilayer. *Nano Lett.* **2007**, *7*, 614−619.
(22) Yang, K.; Ma, Y.-Q. Computer simulation of the translocation of nanoparticles with different shapes across a lipid bilayer. *Nat. Nanotechnol.* **2010**, *5*, 579−583.
(23) Wallace, E. J.; Sansom, M. S. Blocking of carbon nanotube based nanoinjectors by lipids: a simulation study. *Nano Lett.* **2008**, *8*, 2751−2756.
(24) Al-Haik, M. S.; Hussaini, M. Y. Adhesion energy of single-wall carbon nanotube-polyethylene composite: effect of magnetic field. *J. Comput. Theor. Nanosci.* **2006**, *3*, 243−248.
(25) Tanaka, T.; Liu, H. P.; Fujii, S.; Kataura, H. From metal/semiconductor separation to single-chirality separation of single-wall carbon nanotubes using gel. *Phys. Status Solidi RRL* **2011**, *5*, 301−306.
(26) Lustig, S. R.; Jagota, A.; Khripin, C.; Zheng, M. Theory of structure-based carbon nanotube separations by ion-exchange chromatography of DNA/CNT hybrids. *J. Phys. Chem. B* **2005**, *109*, 2559−2566.
(27) Ozawa, H.; Fujigaya, T.; Niidome, Y.; Hotta, N.; Fujiki, M.; Nakashima, N. Rational concept to recognize/extract single-walled carbon nanotubes with a specific chirality. *J. Am. Chem. Soc.* **2011**, *133*, 2651−2657.
(28) Zhu, X. F.; Li, Y. G.; Duan, P. F.; Liu, M. H. Self-assembled ultralong chiral nanotubes and tuning of their chirality through the mixing of enantiomeric components. *Chem.—Eur. J.* **2010**, *16*, 8034−8040.
(29) Mensah, S. Y.; Allotey, F. K. A.; Mensah, N. G.; Nkrumah, G. Differential thermopower of a CNT chiral carbon nanotube. *J. Phys.: Condens. Matter* **2001**, *13*, 5653−5662.
(30) Liang, S. D.; Xu, N. S. Chirality effect of single-wall carbon nanotubes on field emission. *Appl. Phys. Lett.* **2003**, *83*, 1213−1215.
(31) Natsuki, T.; Tantrakarn, K.; Endo, M. Prediction of elastic properties for single-walled carbon nanotubes. *Carbon* **2004**, *42*, 39−45.
(32) Foloppe, N.; MacKerell, A. D. All-atom empirical force field for nucleic acids: I. Parameter optimization based on small molecule and condensed phase macromolecular target data. *J. Comput. Chem.* **2000**, *21*, 86−104.
(33) MacKerell, A. D.; Banavali, N. K. All-atom empirical force field for nucleic acids: II. Application to molecular dynamics simulations of DNA and RNA in solution. *J. Comput. Chem.* **2000**, *21*, 105−120.
(34) Alexander, D.; MacKerell, J.; Banavali, N.; Foloppe, N. Development and current status of the CHARMM force field for nucleic acids. *Biopolymers* **2001**, *56*, 257−265 (Nucleic Acid Sciences section).
(35) MacKerell, A. D., Jr.; Bashford, D.; Bellott, M.; Dunbrack, R. L., Jr.; Evanseck, J. D.; Field, M. J.; Fischer, S.; Gao, J.; Guo, H.; Ha, S.; Joseph-McCarthy, D.; Kuchnir, L.; Kuczera, K.; Lau, F. T. K.; Mattos, C.; Michnick, S.; Ngo, T.; Nguyen, D. T.; Prodhom, B.; Reiher, W. E.; Roux, B.; Schlenkrich, M.; Smith, J. C.; Stote, R.; Straub, J.; Watanabe, M.; Wiórkiewicz-Kuczera, J.; Yin, D.; Karplus, M. All-atom empirical potential for molecular modeling and dynamics studies of proteins. *J. Phys. Chem. B* **1998**, *102*, 3586−3616.
(36) Feller, S. E.; Alexander, D.; MacKerell, J. An improved empirical potential energy function for molecular simulations of phospholipids. *J. Phys. Chem. B* **2000**, *104*, 7510−7515.
(37) Klauda, J. B.; Brooks, B. R.; Alexander, D.; MacKerell, J.; Venable, R. M.; Pastor, R. W. An ab initio study on the torsional surface of alkanes and its effect on molecular simulations of alkanes and a DPPC bilayer. *J. Phys. Chem. B* **2005**, *109*, 5300−5311.
(38) Lopez, C. F.; Moore, P. B.; Shelley, J. C.; Shelley, M. Y.; Klein, M. L. Computer simulation studies of biomembranes using a coarse grain model. *Comput. Phys. Commun.* **2002**, *147*, 1−6.
(39) Shelley, J. C.; Shelley, M. Y.; Reeder, R. C.; Bandyopadhyay, S.; Klein, M. L. A coarse grain model for phospholipid simulations. *J. Phys. Chem. B* **2001**, *105*, 4464−4470.
(40) Zhou, G.; Duan, W.; Gu, B. Electronic structure and field-emission characteristics of open-ended single-walled carbon nanotubes. *Phys. Rev. Lett.* **2001**, *87*, 095504.
(41) Al-Haik, M.; Hussaini, M. Y.; Garmestani, H. Adhesion energy in carbon nanotube-polyethylene composite: effect of chirality. *J. Appl. Phys.* **2005**, *97*, 074306.
(42) Liang, Z. Y.; Gou, J. H.; Zhang, C.; Wang, B.; Kramer, L. Investigation of molecular interactions between (10,10) single-walled nanotube and Epon 862 resin/DETDA curing agent molecules. *Mater. Sci. Eng., A* **2004**, *365*, 228−234.
(43) Allinger, N. L.; Yuh, Y. H.; Lii, J.-H. Molecular Mechanics. The MM3 force field for hydrocarbons. 1. *J. Am. Chem. Soc.* **1989**, *111*, 8551−8566.
(44) Lii, J.-H.; Allinger, N. L. Molecular mechanics. The MM3 force field for hydrocarbons. 2. Vibrational frequencies and thermodynamics. *J. Am. Chem. Soc.* **1989**, *111*, 8566−8575.
(45) Lii, J.-H.; Allinger, N. L. Molecular mechanics. The MM3 force field for hydrocarbons. 3. The van der Waals' potentials and crystal data for aliphatic and aromatic hydrocarbons. *J. Am. Chem. Soc.* **1989**, *111*, 8576−8582.
(46) Dudek, M. J.; Ponder, J. W. Accurate modeling of the intermolecular electrostatic energy of proteins. *J. Comput. Chem.* **1995**, *16*, 791−816.
(47) Rapaport, D. C. *The Art of Molecular Dynamics Simulation*; Cambridge University Press: Cambridge, U.K., 1995.
(48) Leach, A. R. *Molecular Modeling Principles and Applications*, 2nd ed.; Prentice Hall: Essex, England, 2001.
(49) Lopez, C. F.; Nielsen, S. O.; Moore, P. B.; Klein, M. L. Understanding nature's design for a nanosyringe. *Proc. Natl. Acad. Sci. U.S.A.* **2004**, *101*, 4431−4434.